Outputs of Human Walking for Bipedal Robotic Controller Design

Shu Jiang, Shawanee Partrick, Huihua Zhao and Aaron D. Ames

***Abstract*— This paper presents a method to determine outputs associated with human walking data that can be used to design controllers that achieve human-like robotic walking. We consider a collection of human outputs, i.e., functions of the kinematics computed from experimental human data, that satisfy criteria necessary for *human-inspired* bipedal robot control construction. These human outputs are described in a form amendable to controller design through a special class of time based functions—termed *canonical walking functions*. An optimization problem is presented to determine the parameters of this controller that yields the best fit to the human data that simultaneously produces stable robotic walking. The optimal value of the cost function is used as a metric to determine which human outputs result in the most "human-like" robotic walking. The human-like nature of the resulting robotic walking is verified through simulation.**

I. INTRODUCTION

Human walking has been studied extensively in the field of biomechanics and is typically analyzed by decoding the humans' inner kinematics and kinetics, such as muscle functionality [1], [2], ground reaction forces [3], [4] and energy expenditure [5], [6]. The complexity of the human muscle and nervous systems prevents the direct application of research results from biomechanics to robot design since it is difficult to mimic the inner kinematics of human walking in control. Some research has attempted to bridge this gap by determining the inverse kinematics [7] and forward kinematics [8] of human walking, but the complexity of these methods prevent their direct application to robotic control. The methodology of this paper is to approach human walking from the perspective that a control theorist would take when analyzing a complex system: view the human walking system as a "black box". From this viewpoint, the goal becomes: find "outputs" of this black box that characterize the behavior of the system in the simplest form possible. The result is low-dimensional characterization of human walking that can be used to construct controllers that result in human like robotic walking.

With the general methodology of this paper in mind, we seek *outputs* associated with human walking, computed from experimental human walking data, that appear to characterize walking while simultaneously being applicable to bipedal robotic controller design. Criteria are defined for choosing these outputs. The sets of output combinations that satisfy these criteria can be used to construct controllers for bipedal robots. For the chosen outputs, we discover that all the human outputs are accurately described by a linear function of time or the time response to linear mass-spring-damper systems. Due to the simplicity and universality of these functions, we term them *canonical walking functions*. Moreover, unlike other functions of time that could have been used to fit the human output data (polynomials [6] and Bezier series [9]), the form of the canonical human walking functions provides insight into the kinematics of human walking. We are able to conclude that humans appear to act like linear spring-mass-damper systems for the outputs being considered. Utilizing the human outputs and canonical walking functions, for each human output combination we construct a *human-inspired* controller that results in stable human-like bipedal robotic walking. A constrained optimization problem is introduced to compute these parameters, producing the best fit human data while simultaneously yielding robotic walking. The value of the cost function that solves this optimization problem allows us to determine the best output combination. The end result is that we are able to determine the human outputs that yield the most human-like bipedal robotic walking.

Achieving human-like bipedal walking promises to benefit both robotics research and prosthetic device development. Current approaches to bipedal robotic control—such as controlled symmetries [10] and zero moment point regulation [11]—have yet to produce true human-like robotic walking. The hope is that directly using human data, and outputs of human walking, to guide control construction will help to bridge the gap between these methods and true human-like robotic walking. Moreover, human-like robotic walking can be used in prosthetic and orthotic device design and testing [12], [13]. In order for prosthetic and orthotic devices to create normal walking, it is necessary to mimic the behavior of human walking [14]. Most controllers for prosthetic and orthotic devices are implemented by using human data [15].Different sensors are employed to measure energy and force [16], [17]. If human-like bipedal walking is achieved and human walking can be characterized, the force and energy of human walking can be calculated directly from the position data, which will greatly reduce the cost of devices and simplify controller design.

II. HUMAN OUTPUTS

In this section we seek human outputs which can be used to achieve human-like walking in robotic control. Human walking data was collected experimentally. The human outputs computed from the experimental data, are chosen

This work is supported by by NSF grant CNS-0953823 and NHARP award 00512-0184-2009

S. Jiang, H. Zhao and A. D. Ames are with Department of Mechanical Engineering, Texas A&M University, College Station, TX 77843, email: {shujiang,aames,huihuazhao}@tamu.edu

S. Partrick is with the Department of Biomedical Engineering, Texas A&M University, College Station, TX 77843, email: spatrick2012@gmail.com

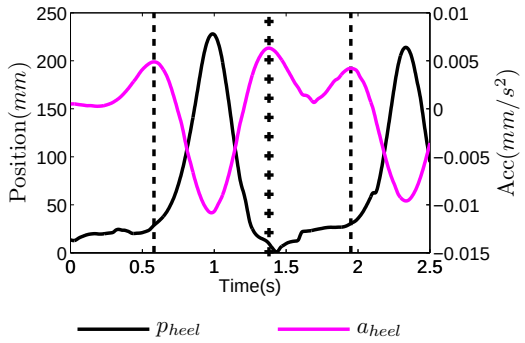

Fig. 1: The position and acceleration data for one heel in z direction. The vertical lines formed by $-$ are the moment the heel lifts the ground. The vertical $+$ line indicates the moment the heel strikes.

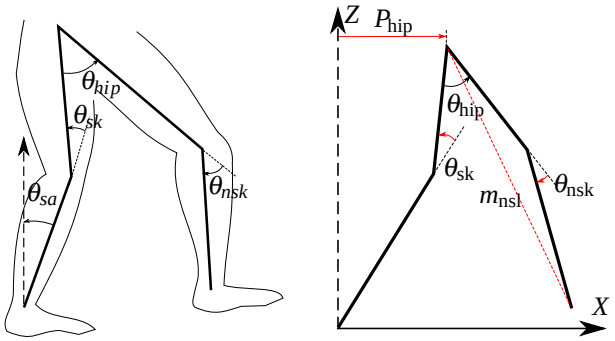

(a) Joint Angles of Human Gait. (b) Human Outputs

Fig. 2: Joint angles of human gait(a) and human outputs(b).

according to criteria necessary for them to be used to construct controllers.

Experimental Setup. The human walking data presented in this paper were collected from a motion capture system as detailed in [18]. Note that the data were collected from two experiments separately. The two experiments have the same setup and were conducted in the same lab. Though the data were collected from two experiments, the results of the analysis are the same, which shows that the data processing algorithm and the experimental results are repeatable. The data used in this paper considers one step cycle ranging from a heel strike of one leg to the following heel strike of the other leg. We distinguish patterns of the heels' behaviors by picking the maximum acceleration in the z direction. Fig. 1 shows how we distinguish the heel pattern. Utilizing this method, we obtain one step cycle of human data. There are two reasons why toe behavior is not considered in this work. First, heel strike represents the main impact from the whole human walking system. Compared with toe behavior, the heel behavior is more important to human walking analysis. Second, the bipedal robot considered in this paper has point feet. Human heel-strike is analogous to foot-strike for such a robot.

Human Outputs. The human outputs we seek should satisfy the following criteria: they (1) are functions of the joint angles, (2) have simple time-based representation, and (3) are mutually exclusive (the decoupling matrix associated with these outputs is non-singular). According to this criteria, we find seven output functions that satisfy conditions (1) and (2), as shown in Fig. 2(b). We will argue these seven outputs appear to be essential to walking.

(1) The x-position of the hip,

$$p_{hip} = L_c \sin(-\theta_{sa}) + L_t \sin(-\theta_{sa} - \theta_{sk}),$$

where L_c is the length of the calf and L_t is length of the thigh.

(2) The linearized hip position,

$$\delta p_{hip} = L_c(-\theta_{sa}) + L_t(-\theta_{sa} - \theta_{sk}),$$

which is the first order terms of the p_{hip} Taylor expansion.

(3) The slope of the non-stance leg, i.e., the tangent of the angle between the z-axis and the line goes through the non-stance ankle and hip, as shown in Fig. 2(b),

$$m_{nsl} = \frac{p^x_{nsa} - p_{hip}}{p^z_{nsa} - p^z_{hip}},$$

where p^z_{hip} is the z position of the hip and p^z_{nsa}, p^x_{nsa} are the z and x position of the non-stance ankle respectively.

(4) The linearized slope of the non-stance leg

$$\delta m_{nsl} = -\theta_{sa} - \theta_{sk} + (\frac{L_c}{L_c + L_t}\theta_{nsk}) - \theta_{hip},$$

which is the first order terms of m_{nsl} Taylor expansion.

(5) The hip angle, which is the angle between the stance thigh and non-stance thigh, θ_{hip}.

(6) The angle of the stance knee, θ_{sk}.

(7) The angle of the non-stance knee, θ_{nsk}.

We consider the linearized form of non-linearized outputs because it is easier to characterize the zero dynamics surface [20] and the linearized outputs have been used to achieve walking experimentally [21], [22]. The outputs can be partitioned into four disjoint sets: $Y_{sa} = \{p_{hip}, \delta p_{hip}\}$, $Y_{hip} = \{m_{nsl}, \delta m_{nsl}, \theta_{hip}\}$, $Y_{sk} = \{\theta_{sk}\}$ and $Y_{nsk} = \{\theta_{nsk}\}$. There is

TABLE I: Physical parameters of each subject in experiments. L_c(mm), L_t(mm), m_c(kg) and m_t(kg) measurements correspond to the lengths described in [18]. Mass distribution is computed according to book [19]

Subject	*Sex*	*Age*	*Ht.*	*Wt.*	m_h	m_t	m_c	L_t	L_c
S_1	M	17	188.5	83.9	56.9	8.4	3.9	49.3	45.1
S_2	M	22	169.5	90.9	61.5	9.1	5.5	40.1	43.5
S_3	M	30	170.5	69.1	46.7	6.9	3.3	43.8	38.1
S_4	M	26	163.5	58.9	39.3	5.9	2.7	38.5	38.2
S_5	F	23	165.5	47.7	32.3	4.8	2.9	39.2	37.6
S_6	F	27	160.0	56.7	38.4	5.7	2.6	46.6	37.1
S_7	M	30	160.5	58.9	40.0	5.9	2.7	38.8	30.4
S_8	M	25	182.0	90.7	61.5	9.1	4.2	49.5	40.1
S_9	M	22	173.0	68.0	46.1	6.8	3.2	59.2	35.6
S_{mean}	*	*	170.3	69.4	47.1	6.9	3.2	45.2	38.1

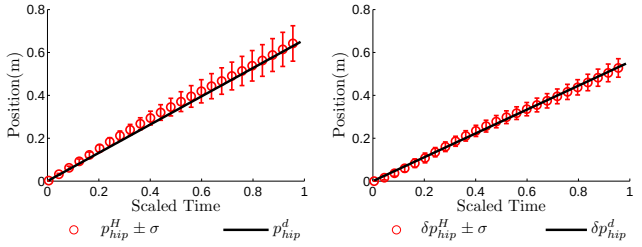

(a) Hip Position (b) Linearized Hip Position

Fig. 3: Human output set Y_{sa} (represented by superscript H) over one step and the canonical walking functions (represented by superscript d) that are fitted to these data.

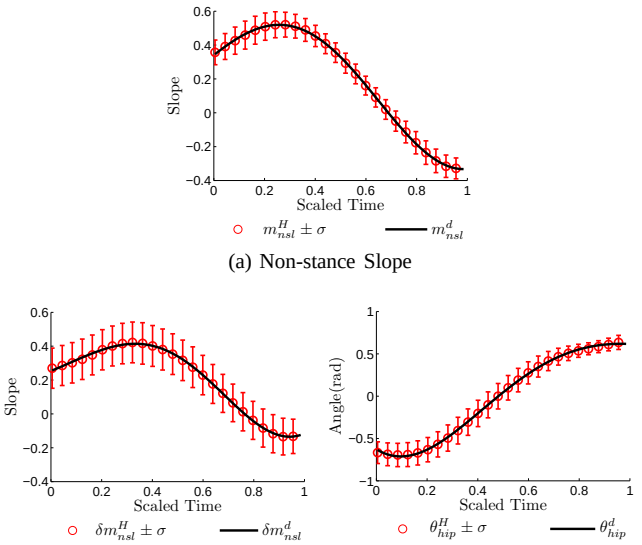

(a) Non-stance Slope

(b) Linearized Non-stance Slope (c) Hip Angle

Fig. 4: Human output set Y_{hip} (circles) over one step and the canonical walking functions (solid lines) that are fitted to these data.

a one-to-one correspondence between the angles and the output sets: Y_{sa} corresponds to θ_{sa}; Y_{hip} corresponds to θ_{hip}; Y_{sk} corresponds to θ_{sk} and Y_{nsk} corresponds to θ_{nsk}. Any combination of the elements between these sets are mutual exclusive, which indicates that the decoupling matrix associated with these outputs is full rank [18]. The end result is 6 total sets of output combinations that satisfy criteria (1)-(3), i.e., six collections of human outputs that can be used to construct controllers for bipedal robots. The mean human outputs are shown in Fig. 3 to 5 along with the error band of one standard deviation. According to [23], outputs that lay within the error bands are considered healthy human walking.

Canonical Walking Functions. To apply the human outputs, which are discrete data, to bipedal robot control, we need to represent the data as functions of time. We propose the following functions (which will be fitted to the human outputs to provide a time-based representation of the human

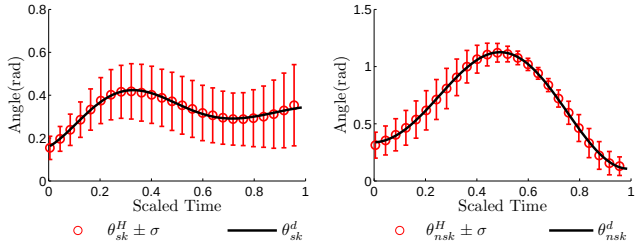

(a) Stance Knee Angle (b) Non-stance Knee Angle

Fig. 5: Human output sets Y_{sk} and Y_{nsk} (circles) over one step and the canonical walking functions (solid lines) that are fitted to these data.

walking data):

$$y_1^H = vt, \tag{1}$$

$$y_2^H = e^{-\alpha_4 t}(\alpha_1 \cos(\alpha_2 t) + \alpha_3 \sin(\alpha_2 t)) + \alpha_5. \tag{2}$$

These functions are termed canonical walking functions, because they appear to represent human outputs universally with a simple form. Equation (1) is fitted to the output elements in the Y_{sa}. Equation (2) is fitted to the other outputs. Note that (2) has the same form as the time response of a linear mass-spring-damper system:

$$y = e^{-\xi \omega_n t}(c_0 \cos(\omega_d t) + c_1 \sin(\omega_d t)) + \bar{g}, \tag{3}$$

where c_0 and c_1 are the initial conditions decided by the initial position $y(0)$ and the initial velocity $\dot{y}(0)$, ξ is the damping ratio and ω_n is the natural frequency, $\omega_d = \sqrt{1-\xi^2}\omega_n$ is the damped frequency and the constant term $\bar{g}$ is the gravity term. Comparing (2) with the time solution of a linear mass-spring-damper systems, we have $\alpha_1 = c_0$, $\alpha_2 = \omega_d$, $\alpha_3 = c_1$, $\alpha_4 = \xi\omega_n$ and $\alpha_5 = \bar{g}$.

The results of the least squares fittings are shown in Figs. 3 – 5 by the solid lines. Table II gives the coefficients along with correlations of each canonical walking function. All the correlations are higher than 0.99. This fact shows that the human outputs are uniformly described with high accuracy by the canonical walking functions. We conclude that human appears to act like linear mass-spring-damper system during walking for the outputs chosen. This result is supported currently in the prosthetic field where spring-damper systems are used to mimic human muscle behaviors.

TABLE II: Parameters of canonical walking functions obtained from fitting.

$y_1^H = vt, \quad y_2^H = e^{-\alpha_4 t}(\alpha_1\cos(\alpha_2 t) + \alpha_3\sin(\alpha_2 t)) + \alpha_5$								
Y	y	v	α_1	α_2	α_3	α_4	α_5	*Cor.*
Y_{sa}	P_{hip}	1.1065	*	*	*	*	*	0.9990
	p^L_{hip}	0.9337	*	*	*	*	*	0.9991
Y_{hip}	m_{nsl}	*	0.1662	7.2502	0.2539	-0.8875	0.1742	0.9999
	m^L_{nsl}	*	0.0117	8.6591	0.1153	-2.1554	0.2419	0.9997
	θ_{hip}	*	-0.9805	6.0632	-0.9366	2.6750	0.3527	0.9997
Y_{sk}	θ_{sk}	*	-0.1739	13.6644	0.0397	3.3222	0.3332	0.9934
Y_{nsk}	θ_{nsk}	*	-0.3439	10.5728	0.0464	-0.8606	0.6812	0.9996

III. CONTROLLER DESIGN

This section uses the human outputs and their time-based representations—the canonical walking functions—to construct a controller that drives the output of the robot to the output of the human. In addition, an optimization problem is introduced to determine the parameters of this controller that provides the best fit of the human walking data while simultaneously yielding stable robotic walking. We consider a 2D bipedal robot model with knee and point feet as described in [18], [21]. The motivation of this is the application of this result to a under-actuated robot AMBER, which has point feet. These result has been translated to AMBER [21] experimentally achieving walking. Finally the point foot approximation has been used in experiments to achieve human-like bipedal walking on a robot with feet [22].

Output Design. Input/output linearization [24] is applied to drive the robotic outputs to human outputs. Based on human outputs, we define the following relative degree one and relative degree two [20] outputs for the bipedal robot model. The actual and desired outputs of relative degree one are defined as:

$$y_1^a(\theta,\dot{\theta}) = dy_{sa}(\theta)\dot{\theta}, \quad y_1^d = v_{hip}, \tag{4}$$

where $y_{sa}(\theta) \in Y_{sa}$. v_{hip} is a constant, i.e., y_{sa} can either be the hip velocity or the velocity of linearized hip position.

The output y_2^a is a vector of the relative degree two outputs. It is defined as

$$y_2^a(\theta) = \begin{bmatrix} y_{hip}(\theta) \\ y_{sk}(\theta) \\ y_{nsk}(\theta) \end{bmatrix}, \quad y_2^d(t) = \begin{bmatrix} y_{hip}^d(t,\alpha_{hip}) \\ y_{sk}^d(t,\alpha_{sk}) \\ y_{nsk}^d(t,\alpha_{sk}) \end{bmatrix}. \tag{5}$$

where $y_{hip} \in Y_{hip}$, $y_{sk} \in Y_{sk}$ and $y_{nsk} \in Y_{nsk}$. The desired output function are $y_{hip}^d(t,\alpha_{hip}) = y_2^H(t,\alpha_{hip})$, $y_{sk}^d(t,\alpha_{sk}) = y_2^H(t,\alpha_{sk})$, and $y_{nsk}^d(t,\alpha_{nsk}) = y_2^H(t,\alpha_{nsk})$ with y_2^H in equation (2). Our goal is to drive $y_1^a \to y_1^d$ and $y_2^a \to y_2^d$ and we start by removing the dependence of time from the desired outputs. The forward hip position is described by $p_{hip} = v_{hip}t$; therefore, for human walking $t \approx p_{hip}/v_{hip}$. This motivates the following parametrization of time:

$$\tau(\theta) = \frac{y_{sa}(\theta) - y_{sa}(\theta^+)}{v_{hip}}, \tag{6}$$

where $y_{sa} \in Y_{sa}$, v_{hip} is a constant of hip velocity or linearized hip velocity and θ^+ is the configuration just after impact. With the parametrized time $\tau(\theta)$, we consider the following outputs:

$$y_1(\theta,\dot{\theta}) = y_1^a(\theta,\dot{\theta}) - y_1^d, \tag{7}$$

$$y_2(\theta) = y_2^a(\theta) - y_2^d(\tau(\theta)). \tag{8}$$

With these outputs, we design a human-inspired controller as presented in [22, Eq.(19)].

Human-Data-Based Optimization. The Partial Hybrid Zero Dynamics (PHZD) based optimization of [18] is employed to determine the parameters of the canonical walking functions that best fit the human data, while still resulting in stable robotic walking. With this goal in mind, we define human-data-based cost as:

$$\text{Cost}_{\text{HD}}(\alpha) = \sum_{k=1}^{K} \sum_{i \in I} \left(\beta_{y_i} (y_i^d(t^H[k],\alpha) - y_i^H[k])^2 \right), \tag{9}$$

where β_{y_i} are the weightings, which are the reciprocal of the maximum and minimum value of the human data for the outputs, $I = \{sa, hip, sk, nsk\}$ are the four outputs which represent the $y_{sa} \in Y_{sa}$, $y_{hip} \in Y_{hip}$, $y_{sk} \in Y_{sk}$ and $y_{nsk} \in Y_{nsk}$.

This cost function is used as a criterion to quantify the differences between robotic walking and human walking. In particular, in [18] a method was developed for expressing the zero dynamics surface, $\mathbf{Z}_\alpha$, and the partial zero dynamics surface, $\mathbf{PZ}_\alpha$, *only* in terms of the parameters α. The optimization problem is thus given as:

$$\alpha^* = \underset{\alpha \in \mathbb{R}^{16}}{\text{argmin}} \ \text{Cost}_{\text{HD}}(\alpha) \tag{10}$$

$$\text{s.t.} \quad \Delta(S \cap \mathbf{Z}_\alpha) \subset \mathbf{PZ}_\alpha \tag{PHZD}$$

where Δ is the reset map, of which the detail definition is given in [21, Eq.(3)]. Note that this optimization only depends on the parameters α, and produces a unique point $[\theta(\alpha), \dot{\theta}(\alpha)] \in S \cap \mathbf{Z}_\alpha$ such that $\Delta(\theta(\alpha), \dot{\theta}(\alpha)) \in \mathbf{PZ}_\alpha$. Moreover, the point $[\theta(\alpha), \dot{\theta}(\alpha)]$ will be the fixed point of a stable periodic orbit, i.e., a stable walking gait. This optimization, therefore, not only produces parameters that best fit the human data, but ensures stable robotic walking and explicitly produces the initial condition for this walking gait.

Simulation Results. A 2D kneed bipedal robot [18] is considered with physical parameters listed in Table I as

TABLE III: Optimization results of each output combination obtained by solving (10)

		$y_1^d = vt, \quad y_2^d = e^{-\alpha_4 t}(\alpha_1 \cos(\alpha_2 t) + \alpha_3 \sin(\alpha_2 t)) + \alpha_5$							
Y	y	v	α_1	α_2	α_3	α_4	α_5	*Cor.*	*Cost*
1	P_{hip}	1.0919	*	*	*	*	*	0.9990	
	m_{nsl}	*	0.1184	6.8404	0.0820	-2.8059	0.2849	0.9951	
	θ_{sk}	*	-0.3152	10.7101	0.2345	6.3638	0.3133	0.9517	
	θ_{nsk}	*	-0.2769	8.3986	0.3287	-0.7328	0.5826	0.9884	1.98
2	P_{hip}	0.9362	*	*	*	*	*	0.9990	
	m_{nsl}^L	*	0.0466	7.7313	0.0713	-3.5520	0.2747	0.9917	
	θ_{sk}	*	-0.3101	11.1149	0.2060	6.2400	0.3157	0.9551	
	θ_{nsk}	*	-0.3300	9.8342	0.1221	-1.0240	0.6392	0.9978	3.05
3	P_{hip}	1.0919	*	*	*	*	*	0.9990	
	θ_{hip}	*	-0.7290	5.4485	-0.0788	0.3504	0.0664	0.9974	
	θ_{sk}	*	-0.2964	10.5414	0.2454	6.4075	0.3147	0.9522	
	θ_{nsk}	*	-0.2727	8.3097	0.3497	-0.6234	0.5800	0.9867	2.08
4	P_{hip}^L	0.9559	*	*	*	*	*	0.9991	
	m_{nsl}	*	0.0923	7.0185	0.0710	-2.9054	0.2391	0.9956	
	θ_{sk}	*	-0.3105	10.7700	0.2329	6.3020	0.3135	0.9537	
	θ_{nsk}	*	-0.3323	9.8612	0.1187	-1.0225	0.6383	0.9978	1.87
5	P_{hip}^L	0.8499	*	*	*	*	*	0.9991	
	m_{nsl}^L	*	-0.0100	8.8926	0.0746	-3.8786	0.2705	0.9963	
	θ_{sk}	*	-0.2354	12.2941	0.1133	4.7734	0.3220	0.9809	
	θ_{nsk}	*	-0.3445	10.1027	0.0963	-0.8205	0.6635	0.9991	2.27
6	P_{hip}^L	0.9268	*	*	*	*	*	0.9991	
	θ_{hip}	*	-0.3975	6.0662	0.0421	-1.2215	-0.1557	0.9972	
	θ_{sk}	*	-0.2234	11.9485	0.1258	4.7811	0.3216	0.9788	
	θ_{nsk}	*	-0.3427	9.7484	0.1541	-0.7001	0.6593	0.9977	1.53

s_{mean}. As stated in section II, the six total human output combinations are considered. The end result is six human inspired controllers for the bipedal robot as listed in TABLE III. The parameters of each controller are obtained by solving the human-data-based optimization problem (10), the results of which are given in Table III. Moreover, the stability of walking is numerically verified by computing the eigenvalues of Poincaré map. All the magnitudes of the eigenvalues are smaller than one as shown in Fig.6, which implies that all walking gaits are stable.

The best output combination is $Y_6 = \{\delta p_{hip}, \theta_{hip}, \theta_{sk}, \theta_{nsk}\}$ since it has the lowest optimization cost. Simulation results of Y_6, as compared against the human data, are given in Fig. 8. The solid lines, which represent the robot outputs, are very close to the red circle lines, which are the human mean outputs. Fig. 7(a) shows the periodic orbit associated with this walking. Fig. 7(b) shows the actual outputs y_i^a and the desired outputs y_i^d over the course of one step; in this figure, it can be seen that hybrid invariance is achieved for the relative degree two outputs (as guaranteed by the partial hybrid zero dynamics optimization (10)). Therefore, the actual and desired outputs of relative degree two agree on value at all times. Fig. 10 is the simulation results of Y_4. Besides comparison between human outputs and robot outputs, there is Fig. 10(a) showing that, while we did not directly attempt to match the joint angles of the robot to those of the human, forcing the robotic outputs to agree with the human outputs results in good agreement between the joint angles as well.

Finally, a comparison of the robotic walking with the human walking is shown in Fig. 9. This implies that the methods proposed in this paper can be applied to achieve human-like walking on bipedal robots, even though they differ from humans in form and structure.

IV. CONCLUSIONS

This paper analyzed human walking by viewing the human walking system as a "black box" and sampling its outputs. Specific human outputs were chosen that appeared to characterize walking, while simultaneously being useful for controller design. To utilize the human outputs for the design of these controllers, canonical walking functions were considered. These time-based functions—which were simply the solution to a mass-spring-damper system—described the human output data with a high degree of accuracy. Human-inspired controllers were then constructed that drive the outputs of the robot to the outputs of the human, and an optimization problem was considered that determined the parameters of this controller that best fit the human data while producing stable robotic walking. The cost function associated with this optimization allows us to determine the best human outputs, i.e., the human outputs that give the most "human-like" robotic walking. Finally, simulation results show the human-like nature of this robotic walking. Future work will be devoted to the experimental realization of this method.

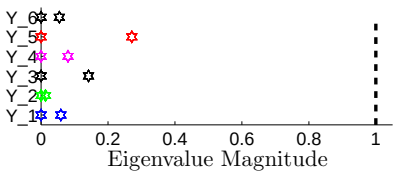

Fig. 6: The magnitudes of eigenvalues associated with the periodic orbits of 6 output combinations

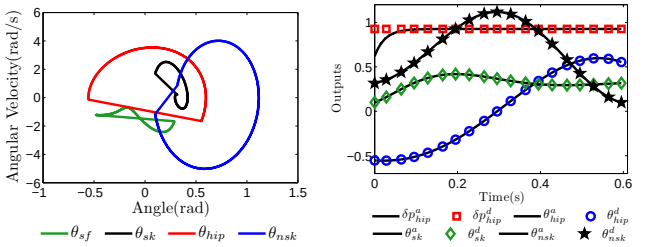

(a) Phase Portraits.

(b) The actual outputs compared to the desired outputs over one step.

Fig. 7: The simulation results of the 2D bipedal robot model with $Y_6 = \{\delta p_{hip}, \theta_{hip}, \theta_{sk}, \theta_{nsk}\}$. The parameters of the controller guarantee the PHZD.

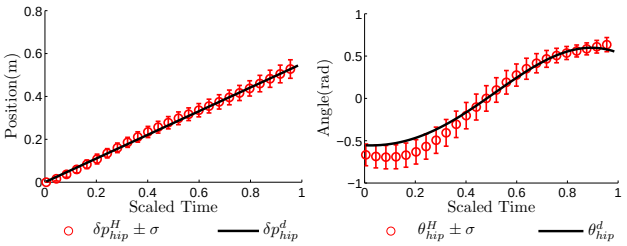

(a) Linearized Hip Posiiton

(b) Hip Angle

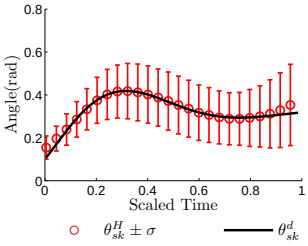

(c) Stance Knee Angle

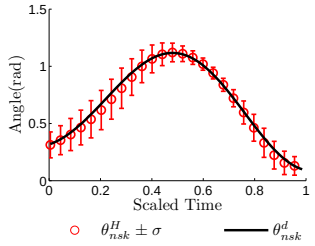

(d) Non-stance Knee Angle

Fig. 8: Desired outputs (solid lines) compared with human outputs (red circles) over one step for Y_6

REFERENCES

[1] D. M. Bojanic, B. D. Petrovacki-Balj, N. D. Jorgovanovic, and V. R. Ilic, "Quantification of dynamic EMG patterns during gait in children with cerebral palsy." *Journal of neuroscience methods*, vol. 198, no. 2, pp. 325–331, June 2011.

[2] M. Cifrek, V. Medved, S. Tonković, and S. Ostojić, "Surface EMG based muscle fatigue evaluation in biomechanics." *Clinical biomechanics (Bristol, Avon)*, vol. 24, no. 4, pp. 327–40, May 2009.

[3] J. R. Watt, J. R. Franz, K. Jackson, J. Dicharry, P. O. Riley, and D. C. Kerrigan, "A three-dimensional kinematic and kinetic comparison of

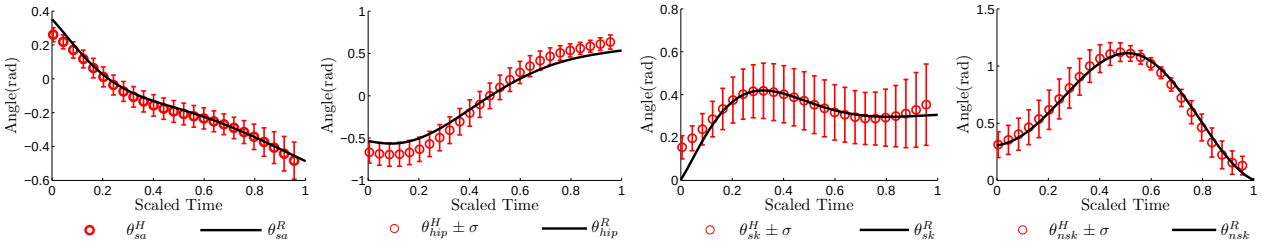

(a) Joint angles of human (circles) compared with associated joint angles of the robotic model (solid lines).

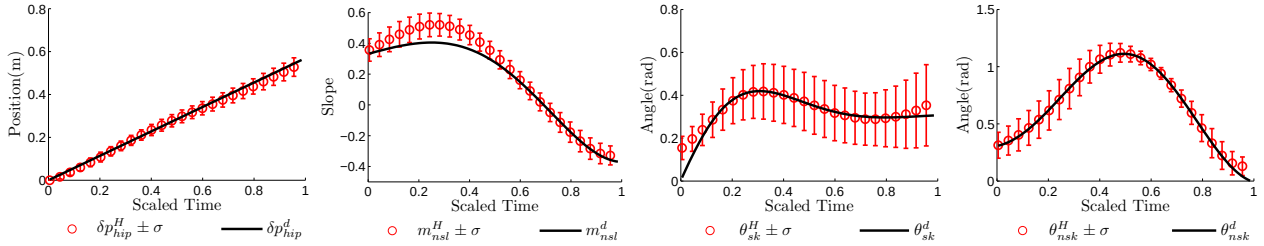

(b) Human outputs (circles) compared with desired outputs (solid lines) of robotic model over one step

Fig. 10: Simulation results for $Y_4 = \{\delta p_{hip}, m_{nsl}, \theta_{sk}, \theta_{nsk}\}$. The error bands are one standard deviations of human data.

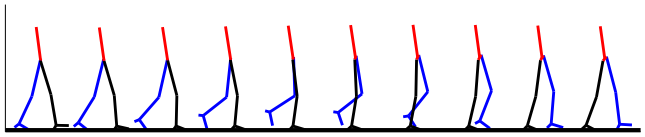

(a) Human walking tiles

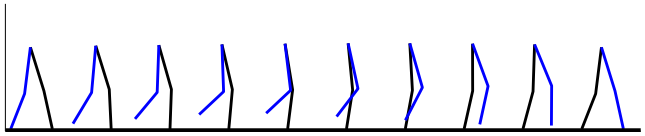

(b) Robotic model walking tiles

Fig. 9: Comparison of human walking and robotic model walking. The robotic model is under the PHZD control with the output combination Y_6.

overground and treadmill walking in healthy elderly subjects." *Clinical biomechanics (Bristol, Avon)*, vol. 25, no. 5, pp. 444–449, June 2010.

[4] A. Y. C. Wong, M. Sangeux, and R. Baker, "Calculation of joint moments following foot contact across two force plates." *Gait & posture*, vol. 31, no. 2, pp. 292–3, Feb. 2010.

[5] D. Rand, J. J. Eng, P.-F. Tang, J.-S. Jeng, and C. Hung, "How active are people with stroke?: use of accelerometers to assess physical activity." *Stroke; a journal of cerebral circulation*, vol. 40, no. 1, pp. 163–168, Jan. 2009.

[6] P. A. Kramer, "The effect on energy expenditure of walking on gradients or carrying burdens." *American journal of human biology : the official journal of the Human Biology Council*, vol. 22, no. 4, pp. 497–507, 2010.

[7] B. Koopman, H. J. Grootenboer, and H. J. de Jongh, "An inverse dynamics model for the analysis, reconstruction and prediction of bipedal walking." *Journal of biomechanics*, vol. 28, no. 11, pp. 1369–76, Nov. 1995.

[8] D. G. Thelen and F. C. Anderson, "Using computed muscle control to generate forward dynamic simulations of human walking from experimental data." *Journal of biomechanics*, vol. 39, no. 6, pp. 1107–1115, Jan. 2006.

[9] E. R. Westervelt, J. W. Grizzle, and D. E. Koditschek, "Hybrid zero dynamics of planar biped walkers," *Automatic Control, IEEE Transactions on*, vol. 48, no. 1, pp. 42–56, 2003.

[10] M. W. Spong and F. Bullo, "Controlled symmetries and passive walking," *Automatic Control, IEEE Transactions on*, vol. 50, no. 7, pp. 1025–1031, 2005.

[11] J. H. Choi and J. W. Grizzle, "Planar bipedal walking with foot rotation," in *American Control Conference*. IEEE, 2005, pp. 4909–4916.

[12] N. Kumar, N. Kunju, A. Kumar, and B. Sohi, "Knowledge base generation and its implementation for control of above knee prosthetic device based on SEMG and knee flexion angle," *International Journal of Biomechatronics and Biomedical Robotics*, vol. 1, no. 2, p. 126, 2010.

[13] M. Popovic, A. Hofmann, and H. Herr, "Angular momentum regulation during human walking: biomechanics and control," in *Robotics and Automation, 2004. Proceedings. ICRA'04. 2004 IEEE International Conference on*, vol. 3. IEEE, 2004, pp. 2405–2411.

[14] R. Torrealba, G. Fernández-López, and J. Grieco, "Towards the development of knee prostheses: review of current researches," *Kybernetes*, vol. 37, no. 9/10, pp. 1561–1576, 2008.

[15] D. Grimes, W. Flowers, and M. Donath, "Feasibility of an active control scheme for above knee prostheses," *Journal of Biomechanical Engineering*, vol. 99, no. 77, p. 215, 1977.

[16] H. Herr and A. Wilkenfeld, "User-adaptive control of a magnetorheological prosthetic knee," *Industrial Robot: An International Journal*, vol. 30, no. 1, pp. 42–55, 2003.

[17] E. C. Martinez-Villalpando, J. Weber, G. Elliott, and H. Herr, "Design of an agonist-antagonist active knee prosthesis," *2008 2nd IEEE RAS & EMBS International Conference on Biomedical Robotics and Biomechatronics*, pp. 529–534, Oct. 2008.

[18] A. D. Ames, "First steps toward automatically generating bipedal robotic walking from human data," *To appear in Lecture notes in Control and Information Science*, 2011.

[19] D. A. Winter, *Biomechanics and Motor Control of Human Movement*, 2nd ed. NY: Wiley-Interscience, May 1990.

[20] E. R. Westervelt, J. W. Grizzle, C. Chevallereau, J. H. Choi, and B. Morris, *Feedback Control of Dynamic Bipedal Robot Locomotion*. Boca Raton: CRC, June 2007.

[21] A. D. Ames, "First steps toward underactuated human-inspired bipedal robotic walking," in *To appear in the IEEE International Conference on Robotics and Automation*.

[22] A. D. Ames, E. A. Cousineau, and M. J. Powell, "Dynamically stable robotic walking with nao via human-inspired hybrid zero dynamics," in *To appear in Hybrid Systems: Computation and Control*.

[23] J. Perry and J. M. Burnfield, *Gait Analysis Normal and Pathological Function*, 2nd ed. Thorofare, New Jersey, United States of America: SLACK Incorporated, 2010.

[24] S. S. Sastry, *Nonlinear Systems: Analysis, Stability and Control*. NY: Springer, June 1999.